

# Multipactor Breakdown in Elliptical Waveguide Carrying Orthogonal Polarizations

Samaneh Esfandiarpour<sup>1</sup> and Ali Frtoanpour<sup>2, \*</sup>

**Abstract**—Multipactor effect is studied in a hollow elliptical waveguide carrying two orthogonal polarization modes, i.e., the fundamental ( $TE_{c11}$ ) and the second ( $TE_{s11}$ ) elliptical waveguide modes. The introduction of a modal equivalent voltage allows defining the standard axial ratio, which characterizes each polarization state of the problem. The RF breakdown threshold is determined as a function of the axial ratio, for various amplitudes, and phases of the two elliptical modes. In particular, the effect of second mode on the RF breakdown threshold of the fundamental mode is studied. The simulations are carried out for different values of the ellipse eccentricity.

## 1. INTRODUCTION

Varieties of microwave systems operating under high power RF signals [1–3] in vacuum are at the risk of multipactor breakdown when a high power electromagnetic wave is applied to a microwave device. Secondary electrons emit from the surface, accelerate and resonate under the applied electromagnetic wave. The multipactor phenomenon has destructive effects on the system performance such as system response degradation, noise level increasing, and waveguide wall heating [4–7]. The study and analysis of multipactor phenomenon has been of interest during the last years. This includes the theory and simulation of multipactor in various types of microwave devices such as high-power microwave components, operating under high-vacuum conditions for satellite communication [8–12], and particle accelerators systems [13, 14].

In particular, it is very important to predict the multipactor RF breakdown threshold of a specific waveguide structure. Thus, a number of microwave structures have been studied during last years in the technical literature. In these studies, the effective electron method has been used to obtain the RF breakdown threshold for several components including rectangular waveguides [15], coaxial transmission lines [16, 17], circular waveguides [18, 19], microstrip lines [20], wedge-shaped rectangular guides [21, 22], elliptical waveguides [23, 24], and dielectric resonator waveguide filters [25]. The details of this technique have been extensively reported in [14] and [22], which basically includes the simultaneous tracking of the finite number of effective electrons trajectories. The next steps in multipactor simulation procedure are electron trajectory computation, and analysis of the secondary electrons generation. The final step is to compute the RF multipactor voltage/power breakdown threshold of a given waveguide structure.

This article focuses on the analysis of multipactor effect in hollow elliptical waveguides. Elliptical guides have been employed for the design of microwave passive components, as narrow-band dual-mode filters [26, 27] and polarizers implemented in circular waveguides [28]. In the research area of accelerator physics, elliptical guides have also been used for the simulation of the LHC (CERN) beam pipe, as reported in [13, 14].

---

Received 1 July 2016, Accepted 14 October 2016, Scheduled 30 October 2016

\* Corresponding author: Ali Frtoanpour (frotanpour@uky.edu).

<sup>1</sup> University of Kentucky, College of Engineering, Electrical and Computer Engineering, 453 FPAT, Lexington, KY 40506-0046, USA.

<sup>2</sup> 177 Chemistry-Physics Building, University of Kentucky, 505 Rose Street, Lexington, Kentucky 40506-0055, USA.

In our previous work [23], we studied the multipactor effect generated by the fundamental  $TE_{c11}$  mode occurring within a hollow elliptical pipe. In this paper, we extend the previous theory including both the fundamental and the second ( $TE_{s11}$ ) elliptical waveguide modes; so, the electron trajectories are then governed by the superposition of the electromagnetic fields of both modes. Moreover, a detailed study of the multipactor onset in terms of the axial ratio and the phase difference between the two modes is presented. For such an analysis, we fix a certain level of power which is proportionally split between the first and second elliptical waveguide modes, observing different multipactor behaviors.

The paper is organized in two sections. In Section 2, we describe the multipactor simulation procedure and electromagnetic fields description; an equivalent voltage is properly defined for each elliptical mode, which allows us to describe each polarization state in terms of a complex axial ratio. Next, in Section 3, we present the numerical results obtained by the simulation.

## 2. MODEL DESCRIPTION

### 2.1. Multipactor Algorithm:

Modeling of a multipactor discharge taking place within an elliptical waveguide requires considering the time evolution of a set of electrons moving under a known electromagnetic fields. The procedure used in this work is based on the concept of the effective electron in context of a Monte-Carlo algorithm, which has been successfully used in technical literature for dealing with this kind of problems, as reported in [17, 20, 21, 23].

The simulations begin with effective electrons launch, initially placed near the center of the elliptical guide. The electron preliminary velocities are assigned according to Maxwell-Boltzmann kinetic energy distribution. Trajectory of each effective electron is determined by solving equation of motion numerically by means of Velocity-Verlet algorithm [29, 30]. This method ensures accuracy and reasonable numerical efficiency. In this article, 350 time steps per RF period are considered in order to obtain convergent electron trajectories.

The secondary yield electron emission (SEY) model formulated in [31] is employed in the Monte-Carlo procedure. At each integration step, we check if the electron strikes the elliptical boundary. If an impact occurs, the SEY functions are computed after considering the initial kinetic energy as well as the incidence angle. The impact location of the electron, the electron velocity, and the SEY value are registered. Then, the effective electron is re-emitted from the impact place with a velocity given by a Gaussian distribution of velocities with a mean value of 4 eV and standard deviation of 2 eV [24]. The launching angle of such an electron is obtained by means of the cosine law distribution [24]. At each period, the multiplicity function for each effective electron formulated by Somersalo [32] is computed. Criteria for multipactor discharge are considered between 40 and 100 consecutive impacts to ensure convergence.

### 2.2. RF Electromagnetic Fields:

Let us consider an elliptical waveguide defined by the semi-major-length  $a$  and semi-minor length  $b$ , which are related through the eccentricity by means of  $e = q/a$ ;  $q$  being the semi-focal distance given by  $q^2 = a^2 - b^2$ . The case of a circular boundary is described by  $e = 0$ , whereas the ellipse degenerates into a straight line when  $e = 1$ . Thus, electron dynamics is referred to a Cartesian reference system placed in the center of the ellipse; the semi-major axis is parallel to the  $x$ -axis, and the semi-minor axis is parallel to the  $y$ -axis. In this scenario, the effective two-dimensional motions of the electrons are tracked by using a non-relativistic motion equation, which is derived by means of the well-known Lorentz force, resulting in

$$\ddot{x} = \frac{-\beta}{m}(E_x + \dot{y}\mu_0 H_z); \quad \ddot{y} = \frac{-\beta}{m}(E_y - \dot{x}\mu_0 H_z) \quad (1)$$

where  $\mu_0$  is the free-space magnetic permeability;  $x = x(t)$  and  $y = y(t)$  are the Cartesian coordinates of each effective electron;  $t$  is time;  $\beta$  and  $m$  are the electron charge and mass at rest, respectively;  $E_x$ ,  $E_y$  and  $H_z$  are the corresponding electric and magnetic field components involved in the problem; the

dot symbol denotes time derivative. Obviously, the Cartesian coordinates of the electrons are restricted to the following relationship:  $(x/a)^2 + (y/b)^2 \leq 1$ .

Here, we consider the excitation of the first two elliptical waveguide modes. For moderate values of the eccentricity,  $e < 0.85$ , these modes are  $TE_{c11}$  and  $TE_{s11}$ , which will be denoted as the first and second modes afterwards. Note that the indices  $c$  and  $s$  denote even and odd solutions, respectively. Also, the total axial magnetic field presented in Eq. (1) is given by the superposition of the magnetic fields provided by each mode  $H_z = H_{z1} + H_{z2}$ . The expressions of these field components can be found, for instance, in [33] by Marcuvitz:

$$H_{z1}(\xi, \eta, z, t) = A_1 C e_1(\xi, \chi_{c11}) c e_1(\eta, \chi_{c11}) \times \cos(\omega t - \beta_1 z + \phi_1) \quad (2a)$$

$$H_{z2}(\xi, \eta, z, t) = A_2 S e_1(\xi, \chi_{s11}) s e_1(\eta, \chi_{s11}) \times \cos(\omega t - \beta_2 z + \phi_2) \quad (2b)$$

where  $\xi$  and  $\eta$  are the radial and angular confocal elliptical coordinates, respectively, which are related with the Cartesian coordinates by  $x = q \cosh \xi \cos \eta$ ,  $y = q \sinh \xi \sin \eta$ ;  $C e_1$  and  $S e_1$  are the radial even and odd Mathieu functions of order 1;  $c e_1$  and  $s e_1$  are the angular even and odd Mathieu functions of order 1;  $\chi_{c11}$  and  $\chi_{s11}$  are the first non-vanishing root of the  $C e_1$  and  $S e_1$  radial Mathieu functions, respectively;  $A_1$  and  $A_2$  are the modal amplitudes; finally,  $f = \omega/(2\pi)$  is the frequency;  $\beta_1$  and  $\beta_2$  are the modal propagation constants;  $\psi = \phi_1 - \phi_2$  is the phase difference between both modes, and the RF period is defined as  $T = 1/f$ . The transverse electric field components  $E_\xi(\xi, \eta, z, t)$  and  $E_\eta(\xi, \eta, z, t)$  can be directly obtained by means of Maxwell's equations, which can be easily transformed into the Cartesian coordinates  $E_x(x, y, z, t)$  and  $E_y(x, y, z, t)$ , as requested in Eq. (1). For simplicity, we consider a two-dimensional model where electrons move in the  $z = 0$  plane.

It is well known that the electric fields of the  $TE_{c11}$  and  $TE_{s11}$  elliptical modes are mutually orthogonal. As a consequence, both modes can be considered as vertical-like and horizontal-like polarization states, respectively (see Figs. 2–12, p. 84 of [34]). Therefore, the tip of the electric field vector maps a polarization ellipse at each point of the  $z = 0$  plane. At this point, it should be emphasized that these sets of ellipses are produced by two orthogonal modes oscillating at the same frequency  $f$ , but we want to remark that these sets of ellipses are not related with the elliptical shape of the waveguide.

In order to normalize the expressions of the considered electric fields in the context of the standard parallel-plate multipactor theory [4] two equivalent voltages are defined by integrating the electric field along both vertical and horizontal main axes of the elliptical guide [24].

$$V_1 = 2 \int_0^b E_y(0, y, 0, 0) dy \quad (3a)$$

$$V_2 = 2 \int_0^a E_x(x, 0, 0, 0) dx \quad (3b)$$

Both equivalent voltages are real and positive if the amplitudes  $A_1$  and  $A_2$  are real and positive. So, in order to describe the polarization state of the elliptical signal propagating along the guide, we define an equivalent axial ratio as follows,

$$AR = \frac{V_2}{V_1} e^{j\psi} \quad (4)$$

$j$  being the complex unit, which is obviously a complex number. The case of  $AR = 0$  represents the existence of the single vertical polarization. Also,  $AR = \pm j$  corresponds to the circular polarization.

Analysis of the second elliptical waveguide mode effect on the multipactor breakdown voltage threshold is the main goal of this work. It is obvious that the inclusion of the second mode introduces additional electromagnetic energy in the system. In order to maintain a constant value of the total injected RF energy during the discharge, we calculate the modal time-average electric energy stored on an elliptical waveguide cross-section ( $CS$ ), which can be expressed as follows

$$W_i = \int_{CS} \frac{1}{4} \epsilon_0 \vec{E}_i \cdot \vec{E}_i^* dS = k_i |V_i|^2; \quad i = 1, 2 \quad (5)$$

in which, the asterisk (\*) signifies the complex conjugate;  $\epsilon_0$  is the electric permittivity of free space;  $E_i$  is the modal electric fields;  $k_i$  are the parameters which depends on both the geometry and the frequency.

It should be emphasized that these constants are equal ( $k_1 = k_2$ ) when the ellipse degenerates into a circle,  $e = 0$  (in this case, the first and second modes are degenerated into the fundamental  $TE_{11}$  circular mode). As a consequence, the total electric energy stored in the system is given by

$$W_{12} = W_1 + W_2 = k_1|V_1|^2 + k_2|V_2|^2 \quad (6)$$

which can be formulated in terms of the magnitude of the axial ratio,

$$W_{12} = |V_1|^2 (k_1 + k_2|AR|^2) \quad (7)$$

Thus, for the single first mode excitation, the electric energy stored by the fundamental mode can be expressed as  $W'_1 = k_1|V'_1|^2$ . Now, if this energy is made equal to the energy stored by the two modes,  $W_{12} = W'_1$ , we find the expressions of the equivalent modal voltages as a function of the magnitude of the axial ratio and the equivalent voltage of the single first mode:

$$|V_1| = \frac{|V'_1|}{\sqrt{1 + (k_2/k_1)|AR|^2}} \quad (8a)$$

$$|V_2| = \frac{|V'_1|}{\sqrt{(1/|AR|^2) + (k_2/k_1)}} \quad (8b)$$

which will be used in the numerical simulations.

### 3. NUMERICAL RESULTS

For the simulations presented in this article, we suppose that the semi-minor axis of the involved elliptical guides is  $b = 1$  mm and that the operation frequency is  $f = 1$  GHz, which means that all the waveguide modes are evanescent. Accordingly, the proposed analysis concerns with use of the elliptical waveguides as an iris, as reported in [20, 21].

Silver is used in the computations of the secondary electrons, which is characterized by the following SEY ( $\delta$ ) parameters (extracted from [6]): first crossover energy,  $W_1 = 30$  eV; maximum value of SEY,  $\delta_{\max} = 2.22$ ; and incident electron energy for  $\delta_{\max}$ ,  $W_{\max} = 165$  eV.

#### 3.1. Multipactor Generated by the Second Elliptical Waveguide Mode

The multipactor discharge generated by the presence of the first elliptical waveguide mode,  $TE_{c11}$ , was detailed in [26]. Now, we have studied the discharge, excited by the second elliptical mode,  $TE_{s11}$ , which leads to similar results to those previously presented for the first mode. In Fig. 1, we show electron trajectories for three different values of the eccentricity  $e = 0.2, 0.4, 0.8$  by observing a typical first order double-surface stable multipactor regime.

In Fig. 2, we compare the RF breakdown voltage threshold for both single waveguide modes using different geometries. As can be observed for  $e = 0.2$  in Fig. 2(a), the presented results are almost

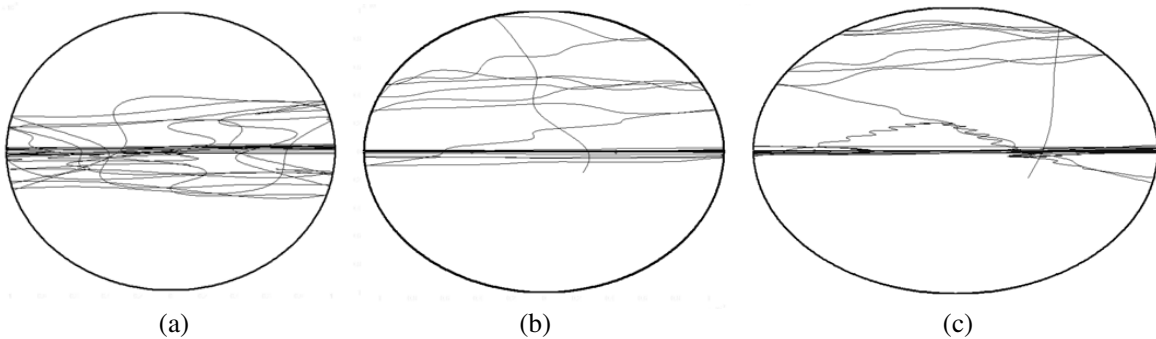


**Figure 1.** Electron trajectories under second mode excitation for 50 impacts. A first-order double-surface multipactor regime is observed in the three plots for a single second elliptical mode excitation.  $f \cdot d = 2$  GHz-mm,  $V_2 = 200$  V. (a)  $e = 0.2$ , (b)  $e = 0.4$ , (c)  $e = 0.8$ .

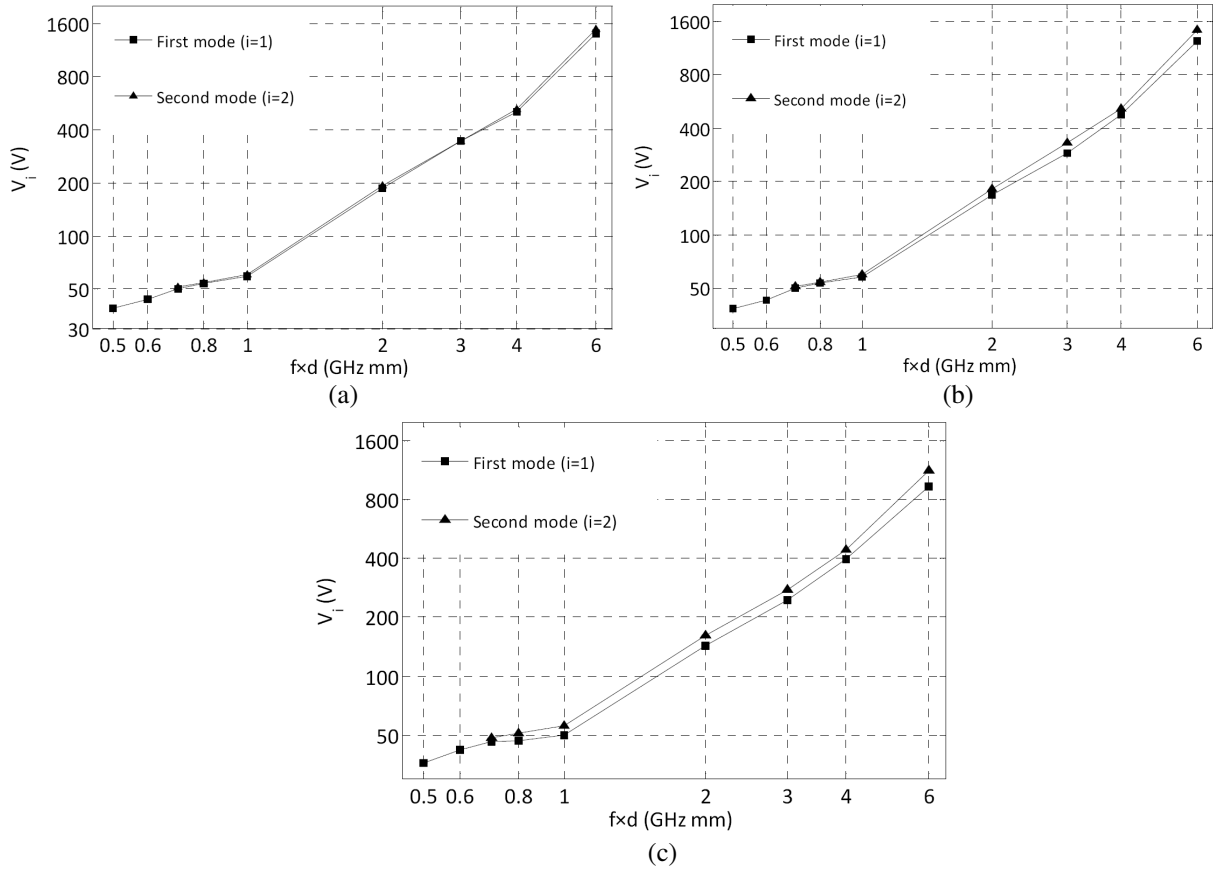


**Figure 2.** RF breakdown voltage threshold for a multipactor discharge excited by the single first ( $TE_{c11}$ ) or second ( $TE_{s11}$ ) elliptical waveguide modes (a)  $e = 0.2$ , (b)  $e = 0.4$ , (c)  $e = 0.8$ .

identical because the elliptical guide is quite similar to the circular one, where the first two modes are degenerated. However, when we increase the value of the eccentricity, the voltage threshold is lower for the first mode than the second mode, because the distance traveled by the electrons under the second mode excitation (2a) is larger than the covered length when the discharge is generated by the first mode (2b), which means an increase of the frequency  $\times$  gap parameter.

### 3.2. Multipactor Generated by Combination of Two Elliptical Waveguide Modes

The main goal of this article is the study of the lowest multipactor harmonics existing in a hollow elliptical guide when the first and second elliptical modes are simultaneously applied. In Fig. 3, we show the RF breakdown voltage threshold for a superposition of both modes as a function of the magnitude of the axial ratio; three different values of phase difference have been considered, and the eccentricity is fixed at  $e = 0.8$ . Three different values of the phase difference have been studied, observing an increase of the threshold for higher values of  $\psi$ . This phenomenon can be understood if we consider that the polarization ellipse created by both modes degenerates into a circle when  $\psi = \pi/2$  and  $|AR| = 1$ . This enhances the dispersion motion of the electron in regard with the linear polarization ( $\psi = 0$ ), shown in Fig. 4. In this figure, electron trajectories are shown for 30 electron impacts considering three different values of phase difference,  $\psi = 0, \pi/4, \pi/2$ . Also, the time difference between consecutive impacts increases when the phase difference rises up from  $\psi = 0$  to  $\psi = \pi/2$ . The average time difference between consecutive impacts is used to calculate the multipactor order, concluding  $\Delta t/T = 0.507$  for  $\psi = 0$ ,  $\Delta t/T = 0.743$  for  $\psi = \pi/4$ , and  $\Delta t/T = 1.03$  for  $\psi = \pi/2$ , which indicates a double-surface first order multipactor in the first case, an hybrid mode in the second one, and a single-surface first order multipactor harmonic for the last case.

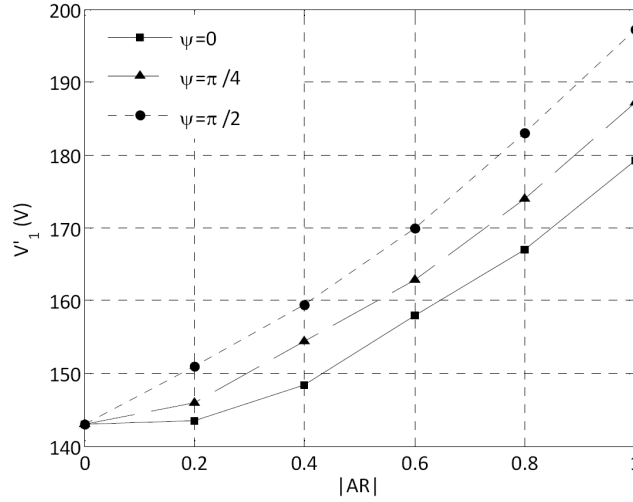


**Figure 3.** RF breakdown voltage threshold for a multipactor discharge excited by the linear combination of the first ( $TE_{c11}$ ) and the second ( $TE_{s11}$ ) elliptical waveguide modes. The eccentricity of the elliptical guide is  $e = 0.8$ . Different values of the phase difference between the modes have been explored.

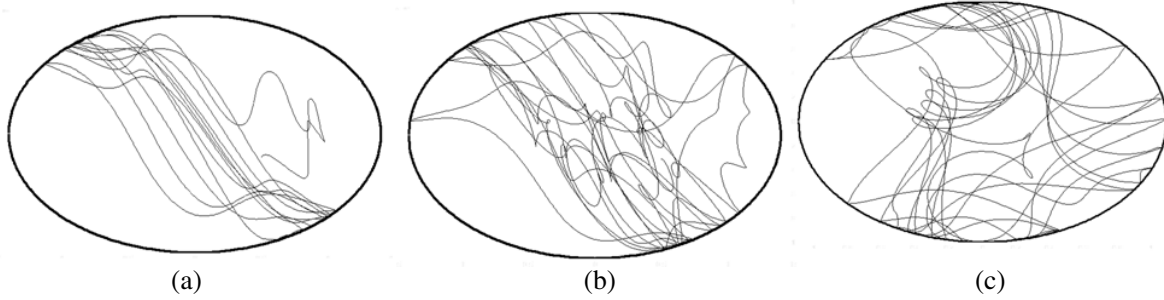


**Figure 4.** Electron trajectories in presence of orthogonal modes for 30 electron impacts,  $E = 0.8$ ,  $b = 1$  mm,  $f = 1$  GHz and  $|AR| = 1$ ; (a)  $\psi = 0$ ,  $V'_1 = 179$  V, (b)  $\psi = \pi/4$ ,  $V'_1 = 186$  V, (c)  $\psi = \pi/2$ ,  $V'_1 = 196.5$  V.

#### 4. CONCLUSION

Multipactor analysis in hollow elliptical waveguide is presented in the presence of second mode of elliptical waveguide,  $TE_{s11}$ . Then, combination of two first modes,  $TE_{c11}$  and  $TE_{s11}$ , is performed to evaluate multipactor breakdown threshold and its behavior under the combination of electromagnetic fields of these two modes. The analysis results are considered for different phase difference values of the electromagnetic fields between the two modes ( $\psi$ ) and various amplitude ratios ( $|AR|$ ). Considering a fixed value of power propagation within the waveguide and increasing the amplitude ratio lead to breakdown threshold increment of the first mode equivalent voltage. Increasing the amplitude ratio means applying less voltage in the semi minor length direction and more voltage in the semi major length direction. So, the vector summation of voltages in those directions rotates toward the semi major length. consequently, the electrons should travel longer distance which means frequency-gap increment causing the increase of breakdown threshold. Moreover, increasing phase difference increases the breakdown threshold. The multipactor order has also been calculated, and the outputs show that multipactor order changes from  $N = 1$  to  $N = 3$  when  $\psi$  changes from zero to  $\pi/2$ , while in between we have seen generation of multipactor hybrid mode.

## REFERENCES

1. Boria, V. E. and B. Gimeno, "Waveguide filters for satellites," *Microwave Magazine, IEEE*, Vol. 8, No. 5, 60–70, 2007.
2. Mallahzadeh, A. R. and S. Esfandiarpour, "Wideband  $H$ -plane horn antenna based on ridge substrate integrated waveguide (RSIW)," *IEEE Antennas and Wireless Propagation Letters*, Vol. 11, 85–88, 2012.
3. Esfandiarpour, S. and A. Frotanpour, "Analysis of a novel V-shape feed line for log-periodic dipole array antenna," *2015 31st International Review of Progress in Applied Computational Electromagnetics (ACES)*, 1–2, Mar. 2015.
4. Hatch, A. J. and H. B. Williams, "Multipactor modes of high-frequency gaseous breakdown," *The Physical Review*, 2nd Series, Vol. 112, No. 3, 681–685, Nov. 1958.
5. Vaughan, J. R. M., "Multipactor," *IEEE Transactions on Electron Devices*, Vol. 35, No. 7, 1172–1180, Jul. 1988.
6. Kishkek, R. A., Y. Y. Lau, L. K. Ang, A. Valfells, and R. M. Gilgenbach, "Multipactor discharge on metals and dielectrics: Historical review and recent theories," *Physics of Plasmas*, Vol. 5, No. 5, 2120–2126, May 1998.
7. Frotanpour, A., G. Dadashzadeh, and M. Shahabadi, "Investigation of multipactor effect on return loss degradation," *5th European Conference on Antennas and Propagation (EUCAP)*, 1739–1742, 2011.
8. Sombrin, J., "Effet multipactor," *CNES Technical Report*, No.83/DRT/TIT/HY/119/T, CNES, Toulouse, France, 1983.
9. Woode, A. and J. Petit, "Diagnostic investigations into the multipactor effect, susceptibility zone measurements and parameters affecting a discharge," Technical Report, ESA/ESTEC Working Paper No. 1556, Noordwijk, The Netherlands, Nov. 1989.
10. *Space Engineering: Multipacting Design and Test*, ESA Publication Division, The Netherlands, ECSS-20-01A, edited by ESA-ESTEC, May 2003.
11. Lara, J., F. Pérez, M. Alfonso, L. Galán, I. Montero, E. Román, and D. Raboso, "Multipactor prediction for on-board spacecraft RF equipment with the MEST software tool," *IEEE Transactions on Plasma Science*, Vol. 34, No. 2, 476–484, Apr. 2006.
12. Anza, S., C. Vicente, D. Raboso, J. Gil, B. Gimeno, and V. E. Boria, "Enhanced prediction of multipaction breakdown in passive waveguide components including space charge effects," *IEEE 2008 International Microwave Symposium*, 1095–1098, Atlanta, Georgia, USA, Jun. 2008.
13. Wang, C., K. Y. Hsieh, L. H. Chang, M. C. Lin, and K. R. Chu, "A tunable reflecting load for multipactor processing of the RF power coupler of a superconducting cavity," *IEEE Transactions on Applied Superconductivity*, Vol. 17, No. 2, 1285–1290, Jun. 2007.
14. Zimmermann, F., "A simulation study of electron cloud instability and beam induced multipacting in the LHC," CERN, Geneva, Switzerland, CERN-LHC-Project-Report-95, Feb. 1997.
15. Semenov, V. E., E. I. Rakova, D. Anderson, M. Lisak, and J. Puech, "Multipactor in rectangular waveguides," *Physics of Plasmas*, Vol. 14, 033501, 2007.
16. Udiljak, R., D. Anderson, M. Lisak, V. Semenov, and J. Puech, "Multipactor in a coaxial transmission line. Part I: Analytical study," *Physics of Plasmas*, Vol. 14, No. 3, 033508, Mar. 2007.
17. Pérez, A. M., C. Tienda, C. Vicente, S. Anza, J. Gil, B. Gimeno, V. E. Boria, and D. Raboso, "Prediction of multipactor breakdown thresholds in coaxial transmission lines for traveling, standing, and mixed waves," *IEEE Transactions on Plasma Science*, Vol. 37, No. 10, 2031–2040, Oct. 2009.
18. Pérez, A. M., V. E. Boria, B. Gimeno, S. Anza, C. Vicente, and J. Gil, "Multipactor analysis in circular wave-guides," *Journal of Electromagnetic Waves and Applications*, Vol. 23, Nos. 11–12, 1575–1583, 2009.
19. Semenov, V. E., N. A. Zharova, D. Anderson, M. Lisak, and J. Puech, "Simulations of multipactor in circular waveguides," *Physics of Plasmas*, Vol. 17, 123–503, 2010.

20. Semenov, V. E., E. I. Rakova, A. G. Sazontov, I. M. Nefedov, V. I. Pozdnyakova, I. A. Shereshevskii, D. Anderson, M. Lisak, and J. Puech, "Simulations of multipactor thresholds in shielded microstrip lines," *Journal of Physics D: Applied Physics*, Vol. 42, 205204, 2009.
21. Semenov, V., E. Rakova, N. Zharova, D. Anderson, M. Lisak, and J. Puech, "Simulations of the multipactor effect in hollow waveguides with wedge-shaped cross section," *IEEE Transactions on Electron Devices*, Vol. 36, No. 2, 488–493, Apr. 2008.
22. Hueso, J., C. Vicente, B. Gimeno, V. E. Boria, S. Marini, and M. Taroncher, "Multipactor effect analysis and design rules for wedge-shaped hollow waveguides," *IEEE Transactions on Electron Devices*, Vol. 57, No. 12, 3508–3517, Dec. 2010.
23. Frotanpour, A., G. Dadashzadeh, M. Shahabadi, and B. Gimeno, "Analysis of multipactor RF breakdown thresholds in elliptical waveguides," *IEEE Transactions on Electron Devices*, Vol. 58, No. 3, 876–881, Mar. 2011.
24. Frotanpour, A., B. Gimeno Martinez, and S. Esfandiarpour, "Multipactor in dual-mode elliptical waveguide," *2015 31st International Review of Progress in Applied Computational Electromagnetics (ACES)*, 2015.
25. Keneshloo, R., G. Dadashzadeh, A. Frotanpour, and M. Okhovvat, "Multipactor analysis in dielectric resonator waveguide filters," *Journal of Communication Engineering*, Vol. 1, 18–24, 2012.
26. Gimeno, B. and M. Guglielmi, "Full wave network representation for rectangular, circular, and elliptical to elliptical waveguide junctions," *IEEE Transactions on Microwave, Theory and Techniques*, Vol. 45, No. 3, 376–384, Mar. 1997.
27. Accatino, L., G. Bertin, and M. Mongiardo, "Elliptical cavity resonators for dual-mode narrow-band filters," *IEEE Transactions on Microwave Theory and Techniques*, Vol. 45, No. 12, 2393–2401, Dec. 1997.
28. Bertin, G., B. Piovano, L. Accatino, and M. Mongiardo, "Full-wave design and optimization of circular waveguide polarizers with elliptical irises," *IEEE Transactions on Microwave Theory and Techniques*, Vol. 50, No. 4, 1077–1083, Apr. 2002.
29. Verlet, L., "Computer experiments on classical fluids. I. Thermodynamical properties of Lennard Jones molecules," *Physical Review*, Vol. 159, No. 1, 98–103, Jul. 1967.
30. Spriter, Q. and M. Walter, "Classical molecular dynamics simulation with the Velocity Verlet algorithm at strong external magnetic fields," *Journal of Computational Physics*, Vol. 152, No. 1, 102–119, Jun. 1999.
31. Vaughan, J. R. M., "A new formula for secondary emission yield," *IEEE Transactions on Electron Devices*, Vol. 36, No. 9, 1963–1967, Sep. 1989.
32. Somersalo, E., P. Yl-Oijala, and D. Proch, "Electron multipacting in RF structures," *Deutsches Elektronen-Synchrotron DESY*, Hamburg, Germany, TESLA Rep., 94-14, 1994.
33. Marcuvitz, N., *Waveguide Handbook*, Peter Peregrinus Ltd., 1993.
34. Collett, E., *Field Guide to Polarization*, SPIE Press Book, 2005.